

Hybrid Modeling and Robust Control for Layer-by-Layer Manufacturing Processes

Adamu Yebi, *Member, IEEE*, and Beshah Ayalew, *Member, IEEE*

Abstract—This paper presents a hybrid system modeling and robust process optimization and control scheme for a layer-by-layer manufacturing process. In particular, the optimization of the layering times is offered as a solution for overcoming the challenge of maintaining through-cure during thick-part fabrication using ultraviolet radiation inputs that are subjected to in-domain attenuation. The layer deposition and curing sequence is modeled as a hybrid system by treating the underlying cure kinetics and the associated thermal process as a continuous dynamics switched by the discrete layering events. The interlayer hold times are taken as the control variables that can be optimally selected to minimize the final cure deviation across all layers. A robust optimization problem is posed that includes the sensitivity of the objective function to process the model parameter uncertainty. By adjoining the hybrid system model and the associated sensitivity constraints to the objective, the necessary conditions of optimality are derived. The advantages of the proposed robust optimization scheme are then demonstrated by simulating a layer-by-layer thick composite laminate fabrication process. It is shown that, compared with the use of nominal optimal layering time control, robust optimal layering time control significantly improves the performance in terms of closely tracking a desired final cure level distribution in the presence of parametric uncertainty.

Index Terms—Additive manufacturing (AM), hybrid modeling of layer-by-layer manufacturing, optimal control of hybrid systems, robust optimization, ultraviolet (UV) curing process.

I. INTRODUCTION

ADDITIVE manufacturing (AM) through layer-by-layer deposition is an actively researched topic for a wide range of applications due to its advantages of reduced processing time, energy use, material waste, and favorable overall environmental impact [1]–[3]. However, its industrial application is still limited due to concerns about product quality. In almost all AM processes, including metal and polymer material deposition, the most common product quality issues are related to geometrical inaccuracy, material shrinkage, layer delamination, and residual stresses [1], [3]–[6]. To overcome some of these product quality defects, a few pragmatic solutions have been proposed. These include an intermediate use of computer numerical control machines [7] and shrinkage

modeling [8] configured to improve the dimensional accuracy. In [9] and [10], closed-loop control has been used for temperature and cladding height control in metal deposition that may indirectly compensate for residual stresses and geometric accuracy.

The product quality can also be improved further through process optimization and control that imbeds process knowledge via high-fidelity modeling of the underlying layer-by-layer process. This can be facilitated by a hybrid system modeling framework, where the addition of each layer constitutes a discrete event on the otherwise continuous dynamics of the underlying physical phenomena in the part buildup process. Although we have not come across prior work, other than our own [13], [14], that models AM processes as hybrid systems, the hybrid systems perspective has been used by others for modeling other manufacturing processes that involve different modes of operation. Specific examples include a steel annealing process, where an individual ingot passes through multiple furnaces with different operating conditions corresponding to certain quality requirements [11] and chemical processes involving different phases of chemical treatment [12].

In [13] and [14], we introduced the hybrid dynamic system modeling perspective for the layer-by-layer ultraviolet (UV) curing process and illustrated how that perspective can be exploited for nominal optimization and optimal control of the process. To begin with, for UV curing thick parts, the need for layer-by-layer part buildup and process optimization is triggered mainly due to the attenuation of UV radiation as it passes through a thick layer of material [15]. To overcome the attenuation challenge and the associated process quality issues, in [13] we proposed a stepped-concurrent layering and curing (SCC) process, where new layers are added before the previous ones cure completely in such a way that each layer is exposed to the full UV intensity only part of the time, and as a result cure level deviations can be minimized in the final product. In SCC, the introduction of a new layer changes the initial conditions of the physical processes and the underlying process dynamics and their spatial domains switch at each discrete layering instant. One can therefore treat the SCC as a multimode hybrid dynamic system, where a mode constitutes the physical processes defined on spatial domains between layer additions. As a layer-by-layer deposition process, SCC has a predefined mode sequence and a growing spatial domain.

In [13], we motivated the need for optimal interlayer hold times for the SCC process and developed a systematic optimization scheme to compute these optimal hold times by treating them as the control inputs. Later in our recent

Manuscript received January 8, 2016; accepted April 3, 2016. Manuscript received in final form April 22, 2016. This work was supported in part by the U.S. National Science Foundation under Grant CMMI-1055254 and in part by the U.S. Department of Energy through the GATE Program under Grant DE-EE0005571. Recommended by Associate Editor M. Prandini.

The authors are with the Clemson University International Center for Automotive Research (CUICAR), Applied Dynamics and Control Group, Greenville, SC 29607, USA (e-mail: ayebi@clemson.edu; beshah@clemson.edu).

Color versions of one or more of the figures in this paper are available online at <http://ieeexplore.ieee.org>.

Digital Object Identifier 10.1109/TCST.2016.2558626

ACC paper [14], we studied the effect of the augmented optimization of both layer-by-layer UV input intensity and interlayer hold times as the control variables. Therein, we considered the complete coupled PDE–ODE UV curing process model for deriving the optimality conditions. The optimization in both our previous works only dealt with model-based optimizations that consider nominal process parameters. However, uncertain model parameters related to cure kinetics such as constants related to reaction order and activation energy affect the utility of the optimization results. In this paper, we build on the work in [14] to address the robustness issue. Specifically, we perform the following.

- 1) We pursue robust optimization that considers the sensitivity of the objective (overall cure level deviation) with respect to process parameter changes.
- 2) We consider a UV curing process model we recently experimentally validated [16].
- 3) We provide detailed derivations for the first-order necessary optimality conditions in the robust hybrid framework for the layer-by-layer process.
- 4) We include new simulation results.

In the broader literature, there exist few works that treat the robustness analysis of theoretical hybrid systems. In [17] and [18], the problem is formulated in a game-theoretic framework that requires a solution of partial differential inequalities. However, the applicability of the abstract results for application-oriented problems has not been demonstrated well. In contrast to this, there is a large volume of work available for application-oriented nonhybrid nonlinear problems [19]–[22]. A minmax performance index that analyzes the worst case performance is commonly adopted for open-loop optimization of nonlinear systems [19]. However, minmax approaches usually handle independent deterministic uncertainties and compute the worst case value, which may have a low probability of occurrence. This often leads to a conservatism, which gives compromised results for more representative uncertainty levels. To improve the minmax approaches, a multiobjective approach has been proposed to add performance indices that account for uncertainty directly [21], [22]. This approach is widely used for final-state optimization problems by defining a robustness term via either the sensitivity [23] or the variance [20] of the nominal performance objective for deterministic and stochastic uncertainty models, respectively. Apart from such direct consideration of robustness analysis for the optimization process, different approaches that include feedback control [24] and online estimation of uncertain parameters [25] can be pursued to accommodate uncertainties. Our review here is limited to application-oriented approaches that incorporate uncertainty into the final-state performance objectives (e.g., minimization of final cure level deviation). More extensive robust performance analyses are available for general nonlinear problems including H_∞ methods [26] and differential geometric approaches [27].

For the UV curing process model, where the uncertain parameters appear as nonlinear functions of the state, we found that the sensitivity approach for robust performance analysis is a suitable candidate over other approaches. This is because it eliminates the need for a disturbance model of the

uncertainty, which is generally difficult to identify or bound accurately for nonlinearly entering parameters. We extend the sensitivity approach for the multiobjective robustness analysis of the hybrid model for the layer-by-layer process. We consider bounded deterministic parameter uncertainties and add a robustness term as a local sensitivity of the objective function. The optimization problem can then be solved as a regular minimization problem by augmenting the auxiliary sensitivity dynamics to the process dynamics [28].

In the literature, there are few works on the optimization or optimal control of hybrid systems whose modes involve PDE models [29], while a lot of work exists for those involving solely ODEs [30]–[33]. In principle, for process dynamics that involve PDEs, one can derive the optimality conditions considering either discretize then optimize or optimize then discretize approaches via adjoint-based techniques [34]. However, the coupling of the PDE and ODE makes the current optimization problem nonstandard. There is some work where the coupled system has been transformed to a standard ODE [35] or PDE [36] optimal control problem, but both transformations add some complexity to the respective governing equations. In [37], the optimality conditions were derived by adjoining the coupled PDE–ODE system directly without using any such transformations. However, they treated a nominal nonhybrid system.

In this paper, we derive the first-order necessary conditions for robust optimality for the hybrid system model of the SCC process by directly adjoining the coupled PDE–ODE constraints of the UV curing process and the robustness sensitivity dynamics. We set the objective function of minimal cure level deviations at the end of the curing process as the objective. The adjoint system and the optimality conditions are then solved to compute the optimal control variables. Since the most significant impact comes from optimizing the layering times as concluded in [14], in this paper, we only consider the layering times as the control variables. We illustrate the effectiveness of the proposed scheme by simulating a layer-by-layer fiberglass composite curing and part buildup process.

The remainder of this paper is organized as follows. Section II gives a generalized 1-D model for a UV curing process and outlines the hybrid modeling formulation. Section III details the derivation of the auxiliary sensitivity dynamics for robustness, as well as the optimality conditions in the hybrid framework. It also presents the numerical algorithm for obtaining optimal solutions. Section IV offers demonstrative numerical simulation results and discussions. Section V gives the conclusions of this paper. Appendixes A and B are provided at the end for the derivation details.

II. HYBRID PROCESS MODEL

A. 1-D UV Curing Process Model

We consider a 1-D process model for UV curing of a single-layer composite laminate. A schematic of the process setup is shown in Fig. 1. The curing process involves exothermic cure reactions (cure kinetics) that cause heat generation and heat transfer through conduction and convection. It also involves the attenuation of UV intensity across the layer in the z -direction according to Beer Lambert’s law [38].

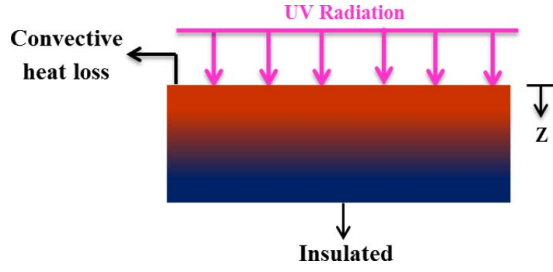


Fig. 1. Schematic of a UV curing process.

Other modeling considerations can be referred from our recent work [16], where a control-oriented model is validated for UV curing of composite laminate or other works that detail this topic [39]. The following coupled PDE–ODE systems, along with the boundary and initial conditions, summarize the process model for UV curing of a single layer:

$$\rho c_p \frac{\partial T(z, t)}{\partial t} = \frac{\partial}{\partial z} \left(k_z \frac{\partial T(z, t)}{\partial z} \right) + v_r \Delta H_r \rho_r \frac{d\alpha(z, t)}{dt} \quad (1a)$$

$$-k_z \frac{\partial T(0, t)}{\partial z} + \vartheta I_0 = h (T(0, t) - T_\infty) \quad (1b)$$

$$\frac{\partial T(l, t)}{\partial z} = 0 \quad (1c)$$

$$T(z, 0) = T_0(z) \quad (1d)$$

$$\frac{d\alpha(z, t)}{dt} = s_0^q \exp(-\lambda p z) I_0^p K_D(\alpha) \times [K_1(T) + K_2(T)\alpha(z, t)] \times (1 - \alpha(z, t)) (\bar{B} - \alpha(z, t)) \quad (1e)$$

$$K_D(\alpha) = \frac{1}{1 + \exp(\xi(\alpha(z, t) - \alpha_c))} \quad (1f)$$

$$K_1(T) = A_1 \exp\left(\frac{-E_1}{RT_{\text{abs}}(z, t)}\right) \quad (1g)$$

$$K_2(T) = A_2 \exp\left(\frac{-E_2}{RT_{\text{abs}}(z, t)}\right) \quad (1h)$$

$$\alpha(z, 0) = \alpha_0(z) \quad (1i)$$

where ρ and c_p are the density and specific heat capacity of the composite laminate, respectively; k_z is the thermal conductivity of the laminate in the z -direction; $T(z, t)$ is the temperature distribution at depth z and time t ; v_r is the volumetric fraction of resin in the composite matrix; ρ_r is the density of resin; ΔH_r is the polymerization enthalpy of resin conversion; ϑ is the absorptivity constant of the UV radiation at the boundary; I_0 is the UV input intensity at the surface; h is the convective heat transfer at the top boundary; l is the thickness of a single layer and T_∞ is the constant ambient temperature; $d\alpha(z, t)/dt$ is the rate of cure conversion (rate of polymerization); s_0 is the photoinitiator concentration; p and q are constant exponents; λ is the absorption coefficient in the resin plus fiber; \bar{B} is the constant parameter related to reaction orders; ξ is the diffusion constant; α_c is the critical value of cure level; A_1 and A_2 are pre-exponential rate constants; E_1 and E_2 are activation energies; R is the gas constant and $T_{\text{abs}}(z, t)$ is the absolute temperature in Kelvin; and $\alpha(z, t)$ is the cure level/state distribution.

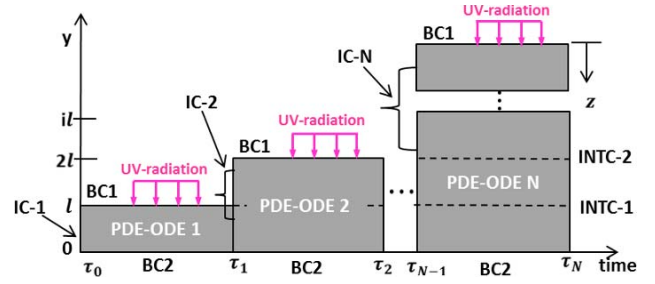


Fig. 2. Hybrid system formulation of the layer-by-layer curing process.

Note that in the cure kinetics model above (1e), we added the diffusion-controlled effect model (1f) to account for the retardation of cure propagation after a certain critical cure level due to restriction of the species diffusion [39]. This effect is neglected in our previous work.

B. Formulation of a Layer-by-Layer UV Curing Process as a Hybrid System

Before posing the control of the layer-by-layer manufacturing process as an optimization problem, we take a closer look at the nature of the process dynamics. In a layer-by-layer UV curing process, as a new layer is introduced for curing, the spatial domain, initial conditions, and boundary conditions change, resulting in a different process dynamics. The layer addition can be treated as a switch of the process mode from one to another. This mode switch represents a discrete event on the otherwise continuous curing process with its associated thermal evolution and cure-reaction phenomena. This makes the layer-by-layer curing process a natural externally switched hybrid system. This hybrid system view of the layer-by-layer curing process is depicted schematically in Fig. 2. In the following, a mode represents the state dynamics before the addition of a new layer. The first mode (Mode 1) has only one layer, and all other modes have more, in increasing numbers, as shown. The mode switching times are denoted by τ_1 through τ_N . In this hybrid system view, the switching/layering times are control variables that can be manipulated for a desired effect, in this case, for minimization of the cure level deviations in a multilayer part.

For this hybrid system realization of the layer-by-layer curing process, the following observations and assumptions can be made.

- 1) At each mode switch (layer addition), from mode i to the next mode $i + 1$, the spatial domain grows and the initial conditions of the mode (IC) change from $IC - i$ to $IC - i + 1$.
- 2) The process dynamics in mode i can be treated as a single coupled PDE–ODE system with the introduction of an interface condition (INTC) that captures the heat transfer between the fresh layer and the layers already in the curing process. The INTC for the curing process is defined in (4).
- 3) The boundary condition (BC) of the top convective (BC1) and the bottom insulation (BC2) are kept the same for all the modes.

4) Since one can only add layers, the order of the mode switching (switching sequence) is fixed, sequential, and known.

5) All of the mode switching times included in the ordered vector $[\tau_1, \dots, \tau_N]'$ can be selected independently.

Note that in Fig. 2, the y -axis indicates the increasing spatial domain with layer addition from the bottom to the top, while the z -axis indicates the direction of UV attenuation. The UV source is at the top.

Denoting the thickness of the part after the i th layer is added by il and introducing a coordinate transformation $y = il - z$ between the global y -axis and the local z -axis, and introducing notations $T_y^i(yt)$, $T_y^i(yt)$, $T_{yy}^i(yt)$, and $\alpha^i(yt)$ for $\partial T^i(yt)/\partial t$, $\partial T^i(yt)/\partial y$, $\partial^2 T^i(yt)/\partial y^2$ and $\partial \alpha^i(yt)/\partial t$, respectively, the state evolution for mode i in the time interval, $t \in [\tau_{i-1}, \tau_i]$ takes the form

$$T^i(y, t) = aT_{yy}^i(y, t) + b(y)f^i(T^i(y, t), \alpha^i(y, t), \theta) \quad \text{in } \Omega_\tau^i \quad (2a)$$

$$T_y^i(il, t) + eI_0 = c(T^i(il, t) - T_\infty) \quad \text{on } \Gamma_1^i \quad (2b)$$

$$T_y^i(0, t) = 0 \quad \text{on } \Gamma_2^i \quad (2c)$$

$$\alpha^i(y, t) = d(y)f^i(T^i(y, t), \alpha^i(y, t), \theta) \quad \text{in } \Omega_\tau^i \quad (2d)$$

where both the temperature state $T^i(y, t)$ and cure state $\alpha^i(y, t)$ evolve in the spatiotemporal domain defined by $\Omega_\tau^i = [0, il] \times [\tau_{i-1}, \tau_i]$. The boundary conditions are also defined on $\Gamma_1^i = \{il\} \times [\tau_{i-1}, \tau_i]$, and $\Gamma_2^i = \{0\} \times [\tau_{i-1}, \tau_i]$. The nonlinear function f^i is

$$\begin{aligned} f^i(T^i(y, t), \alpha^i(y, t), \theta) \\ = I_0^p K_D^i(\alpha) \times \{K_1^i(T) + K_2^i(T)\alpha^i(y, t)\} \\ \times (1 - \alpha^i(y, t))(\bar{B} - \alpha^i(y, t)) \quad \text{in } \Omega_\tau^i \end{aligned} \quad (3)$$

where $\theta \in \mathfrak{R}^m$ is a vector of uncertain parameters and $d(y) = s_0^q \exp(-\lambda p(il - y))$, $b(y) = d(y)(v_r \Delta H_r \rho_r / \rho c_p)$, $a = k_z / \rho c_p$, $c = h / k_z$ and $e = \vartheta / k_z$; K_D , K_1 and K_2 are given in (1f)–(1h). In the following analysis, for brevity, we use $f^i(T^i, \alpha^i, \theta)$ instead of $f^i(T^i(y, t), \alpha^i(y, t), \theta)$, dropping the spatial and temporal indices of the state. Note that in (2), the process input I_0 is treated as a constant parameter and the layering times ($\tau_i \in \mathfrak{R}^+$, $i = 1, \dots, N$) are the control variables to be optimized. Note that the feasible layering times must satisfy the sequence $0 \leq \tau_0 < \tau_1 < \dots < \tau_N < \infty$.

For the UV curing process, the main uncertain parameters include the cure kinetics parameter constants $\theta = [E_1, E_2, \bar{B}]'$. To avoid confusion with the temperature state T , the transpose of a vector is denoted by $[\cdot]'$ instead of the usual $[\cdot]^T$.

For two or more layers, at the interface of new and earlier layers, the INTCs at $i = 1, 2, \dots, N - 1$ are defined as

$$[k_z T_y^i(il, t)]_{\text{new layer}} = [k_z T_y^i(il, t)]_{\text{previous layer}} \quad (4a)$$

$$[T^i(il, t)]_{\text{new layer}} = [T^i(il, t)]_{\text{previous layer}} \quad (4b)$$

At each switching time τ_i , $i = 1, 2, \dots, N - 1$, the transition to the new mode defines the new initial conditions for the next mode. This is described compactly for both the temperature and cure state by

$$\chi^{i+1}(y, \tau_i^+) = F^i(\chi^i(y, \tau_i^-), \chi_0(y)) \quad (5)$$

where $\chi = [T, \alpha]'$ is the augmented state of temperature and cure level, $\chi^i(y, \tau_i^-)$ and $\chi^{i+1}(y, \tau_i^+)$ are the left-hand and right-hand limit values of both the temperature and cure level states in mode i and mode $i + 1$, respectively, at the switching time τ_i , and $\chi_0(y)$ is the initial state at initial time τ_0 . $F^i : \Omega^i \rightarrow \Omega^{i+1}$ is the mode transition operator for both the states at switching time τ_i defined over $\Omega^i \in [0, il]$. Note that both the states coexist in the spatial domain in all modes.

To give a particular example of the mode transition operator for this application, the starting temperature for the interface in the new mode is taken as the average temperature at the interface of the new layer and the layer in the curing process at the switching time τ_i . The cure state at the interface is taken as that of the cure state already in the curing process, because cure conversion is an irreversible process. For all other locations in the domain away from the interfaces that were already being cured (all the previous layers), the initial values of the temperature and cure states in the new mode take their values from the end of the previous mode. Of course, the initial value of all the state elements corresponding to the locations in the new layer will take on ambient conditions.

For example, for the temperature state mode transition operator

$$\begin{aligned} F^i(\chi^i(y, \tau_i^-), \chi_0(y)) \\ = \begin{cases} \chi^i(y, \tau_i^-), & 0 \leq y < il \\ \frac{1}{2}(\chi^i(y, \tau_i^-) + \chi_0(y)), & y = il \\ \chi_0(y), & il < y \leq (i+1)l. \end{cases} \end{aligned} \quad (6)$$

For the cure state, the only change from (6) is at the interface node $y = il$, $F^i(\chi^i(y, \tau_i^-), \chi_0(y)) = \chi^i(y, \tau_i^-)$.

Equations (2)–(6) complete the hybrid system formulation for the layer-by-layer UV curing process.

III. ROBUST OPTIMAL CONTROL OF THE HYBRID SYSTEM

For the hybrid system described by (2)–(5), the optimal control problem can be posed as one of finding the optimal switching time vector $u = [\tau_1, \dots, \tau_N]'$ that minimizes a cost function of the following form:

$$J(u, \theta) = \int_{\Omega}^N g(\chi^N(y, \tau_N^-), \theta) dy + \sum_{i=1}^{N-1} \gamma^i(\tau_i^-) \quad (7)$$

where g is a terminal cost at final time τ_N and $\gamma^i(\tau_i^-)$ is the cost associated with switching at τ_i . The initial time τ_0 and the state $\chi(y, \tau_0)$ are assumed fixed, while the final time τ_N and the state $\chi(y, \tau_N^-)$ are free to be optimized. θ is again the uncertain parameter vector.

For the nominal process optimization we treated in [14], the optimal cost function in (7) is effectively computed by fixing θ at its nominal value $\bar{\theta}$. In the presence of uncertainty, which is the case we treat in this paper, the cost function in (7) is modified to include a robustness term to account for parameter variations. The modified cost functions will have two parts: a part that defines the performance objective with nominal parameters and a part that defines the variation/or sensitivity of the objective to parameter changes. It is written as [28]

$$J_R(u, \theta) \triangleq J(u, \bar{\theta}) + \beta J_\theta(u, \bar{\theta}) [J_\theta(u, \bar{\theta})]' \quad (8)$$

where $\beta \geq 0$ is considered as a robustness measure that defines a tradeoff between the nominal performance and the risk due to uncertainty; and $J_\theta(u, \bar{\theta})$ is the first moment sensitivity term defined as

$$J_\theta(u, \bar{\theta}) \triangleq \left. \frac{\partial J(u, \theta)}{\partial \theta} \right|_{\theta=\bar{\theta}}. \quad (9)$$

For $\beta > 0$, conventional optimization techniques cannot be used directly because the modified cost function $J_R(u, \theta)$ contains sensitivity terms that are functions of states (e.g. $\partial \chi^N(y, \tau_N^-)/\partial \theta$) but are not explicit in the state dynamics. To solve the robust optimization problem, we first construct the auxiliary dynamics for the system sensitivity.

A. Derivation of System Sensitivity

To obtain a characterization of the sensitivity of the hybrid system given in (2)–(5) to the uncertain parameter vector θ , we assume that both f and g are continuously differentiable and f is twice continuously differentiable. Following the forward sensitivity analysis approach from [40], we derive the auxiliary dynamics that defines the system sensitivity in our hybrid framework to be as follows (for $j = 1, \dots, m$):

$$S_t^{T^i, j}(y, t) = a S_{y^i}^{T^i, j}(y, t) + b(y) f^{si}(T^i, \alpha^i, S^{T^i, j}, S^{ai, j}, \theta) \text{ in } \Omega_\tau^i \quad (10a)$$

$$S_y^{T^i, j}(il, t) = c S^{T^i, j}(il, t) \text{ on } \Gamma_1^i \quad (10b)$$

$$S_y^{T^i, j}(0, t) = 0 \text{ on } \Gamma_2^i \quad (10c)$$

$$S_t^{ai, j}(y, t) = d(y) f^{si}(T^i, \alpha^i, S^{T^i, j}, S^{ai, j}, \theta) \text{ in } \Omega_\tau^i \quad (10d)$$

where the nonlinear function f^{si} is

$$f^{si}(T^i, \alpha^i, S^{T^i, j}, S^{ai, j}, \theta) = f_T^i(T^i, \alpha^i, \theta) S^{T^i, j}(y, t) + f_\alpha^i(T^i, \alpha^i, \theta) S^{ai, j}(y, t) \text{ in } \Omega_\tau^i. \quad (11)$$

The following notations are adopted: $S^{T^i, j} = \partial T^i / \partial \theta_j$, $S^{ai, j} = \partial \alpha^i / \partial \theta_j$, $f_T^i = \partial f^i / \partial T^i$, $f_\alpha^i = \partial f^i / \partial \alpha^i$ and $f_\theta^{i, j} = \partial f^i / \partial \theta_j$. Note that the dynamics in (10) are derived considering the sensitivity of the state dynamics to variation of one parameter at a time ($\theta_j, j = 1, \dots, m$).

Similarly, the sensitivity of the INTC in (4) and the mode transition operators in (5) take the forms in (12) and (13), respectively.

Sensitivity of Interface Condition (INTC):

$$[k_z S_y^{T^i, j}(il, t)]_{\text{new layer}} = [k_z S_y^{T^i, j}(il, t)]_{\text{previous layer}} \quad (12a)$$

$$[S^{T^i, j}(il, t)]_{\text{new layer}} = [S^{T^i, j}(il, t)]_{\text{previous layer}}. \quad (12b)$$

Sensitivity of Mode Transition Operators:

$$S^{\chi^{i+1, j}}(y, \tau_i^+) = F_\chi^i(\chi^i(y, \tau_i^-), \chi_0(y)) S^{\chi^i, j}(y, \tau_i^-) \quad (13)$$

where $F_\chi^i = \partial F^i / \partial \chi^i$.

Neglecting the switching cost for our particular application problem of the layer-by-layer UV curing process (assuming instantaneous and equal cost layering operations), the robust optimization of the hybrid system is posed as

$$\min_u \left[\int_\Omega^N g(\chi^N(y, \tau_N^-), \bar{\theta}) dy + \sum_{j=1}^m \beta_j \left[\int_\Omega^N \frac{\partial g(\chi^N(y, \tau_N^-), \bar{\theta})}{\partial \chi^N} S^{\chi^N, j}(y, \tau_N^-) \right]^2 \right] \quad (14)$$

s.t. (2), (4), (5), (10), (12), and (13)

where $S^{\chi^N, j}(y, \tau_N^-) = \partial \chi^N(y, \tau_N^-) / \partial \theta_j$.

B. Optimality Conditions

In the literature, for hybrid/switching systems, a hierarchical decomposition (or two-stage optimization) method is often used to solve a generic optimal control problem that involves optimal switching sequence, optimal switching instants (switching time), and optimal continuous inputs [30], [32], [41]. In [41], stage 1 is posed as an optimization problem of both the continuous input and switching instants, while stage 2 solves the optimal switching sequence. Then, stage 1 is further decomposed into two suboptimizations, where the first one solves the optimal continuous input for given switching instants and switching sequence using the variational approach, while the second one solves for the optimal switching instants by posing the problem as a nonlinear optimization problem. In [31] and [42], for a predefined switching sequence, the variational approach is directly used to solve both the optimal continuous inputs and the switching instants simultaneously by defining perturbations over the optimization variables without decomposing the optimization problem. In [43] and [44], a direct differentiation of the cost function is used to approximate the derivative of the cost function with respect to switching instants to set up a numerical algorithm for the optimal switching instants. In this paper, given the predefined switching sequence and constant continuous input of UV radiation over all the modes, we found the classical variational method outlined in [45] to be more straightforward to apply and to solve the robust optimal switching instants (layering times), given the hybrid realization of the SCC process described by the coupled PDE–ODE dynamics in each mode.

In order to derive the necessary conditions for optimality, we first adjoin the dynamic constraint of the process dynamics (2) and system sensitivity (10), and the corresponding transition constraints (5) and (13) to the cost function defined in (14) using Lagrange multipliers $\bar{p}^{T^i}(y, t)$ for the temperature state equation, $\bar{q}^{ai}(y, t)$ for the cure level state equation, $\bar{p}^{si, j}(y, t)$ for the sensitivity dynamics of temperature, $\bar{q}^{si, j}(y, t)$ for the sensitivity dynamics of cure level, $\mu^i(y, \tau_i^-)$ for the transition constraint, and $\mu^{si, j}(y, \tau_i^-)$ for the sensitivity transition constraint. The first-order necessary conditions for optimality are stated here. The derivation is detailed in Appendix A.

1) *Necessary Conditions:* Modeling the layer-by-layer curing process as a hybrid system of the form (2)–(5) and deriving auxiliary sensitivity dynamics of the form in (10)–(13), an extremum to the cost defined in (14) can be achieved

by choosing a control variable u that satisfies the following conditions.

- a) For $t \in [\tau_{i-1}, \tau_i]$, the adjoint dynamics of the coupled PDE–ODE form the following.

Adjoint equations for the hybrid process dynamics

$$\begin{aligned} \bar{p}_t^{Ti}(y, t) &= -a \bar{p}_{yy}^{Ti}(y, t) - \Upsilon^i(\bar{p}^T, \bar{q}^\alpha) \\ &\times f_T^i(T^i, \alpha^i, \theta) - \sum_{j=1}^m \{ \Upsilon^{si,j}(\bar{p}^s, \bar{q}^s) \\ &\times f_T^{si}(T^i, \alpha^i, S^{Ti,j}, S^{\alpha i,j}, \theta) \} \text{ in } \Omega_\tau^i \end{aligned} \quad (15a)$$

$$\bar{p}_y^{Ti}(il, t) = c \bar{p}^{Ti}(il, t) \text{ on } \Gamma_1^i \quad (15b)$$

$$\bar{p}_y^{Ti}(0, t) = 0 \text{ on } \Gamma_2^i \quad (15c)$$

$$\begin{aligned} \bar{q}_t^{ai}(y, t) &= -\Upsilon^i(\bar{p}^T, \bar{q}^\alpha) f_\alpha^i(T^i, \alpha^i, \theta) \\ &- \sum_{j=1}^m \{ \Upsilon^{si,j}(\bar{p}^s, \bar{q}^s) f_\alpha^{si}(T^i, \alpha^i, S^{Ti,j}, S^{\alpha i,j}, \theta) \} \text{ in } \Omega_\tau^i \end{aligned} \quad (15d)$$

where $\Upsilon^i(\bar{p}^T, \bar{q}^\alpha) = b(y) \bar{p}^{Ti}(y, t) + d(y) \bar{q}^{ai}(y, t) f_\alpha^i = \partial f^{si} / \partial \alpha^i$, $\Upsilon^{si,j}(\bar{p}^s, \bar{q}^s) = b(y) \bar{p}^{si,j}(y, t) + d(y) \bar{q}^{si,j}(y, t)$, and $f_T^{si} = \partial f^{si} / \partial T^i$.

Adjoint equations for auxiliary sensitivity dynamics for $j = 1, 2, \dots, m$

$$\begin{aligned} \bar{p}_t^{si,j}(y, t) &= -a \bar{p}_{yy}^{si,j}(y, t) - \Upsilon^{si,j}(\bar{p}^s, \bar{q}^s) \\ &\times f_T^{si}(T^i, \alpha^i, \theta) \text{ in } \Omega_{i\tau} \end{aligned} \quad (16a)$$

$$\bar{p}_y^{si,j}(il, t) = c \bar{p}^{si,j}(il, t) \text{ on } \Gamma_1^i \quad (16b)$$

$$\bar{p}_y^{si,j}(0, t) = 0 \text{ on } \Gamma_2^i \quad (16c)$$

$$\bar{q}_t^{si,j}(y, t) = -\Upsilon^{si,j}(\bar{p}^s, \bar{q}^s) f_\alpha^i(T^i, \alpha^i, \theta) \text{ in } \Omega_{i\tau}. \quad (16d)$$

- b) Boundary conditions at $t = \tau_N$

$$\bar{p}^{TN}(y, \tau_N^-) = \psi_T(\bar{\chi}^N(y, \tau_N^-), \theta) \quad (17a)$$

$$\bar{q}^{TN}(y, \tau_N^-) = \psi_\alpha(\bar{\chi}^N(y, \tau_N^-), \theta) \quad (17b)$$

$$\bar{p}^{sN,j}(y, \tau_N^-) = \psi_{S^T}(\bar{\chi}^N(y, \tau_N^-), \theta) \quad (17c)$$

$$\bar{q}^{sN,j}(y, \tau_N^-) = \psi_{S^\alpha}(\bar{\chi}^N(y, \tau_N^-), \theta) \quad (17d)$$

where $\psi_{\bar{\chi}}(\bar{\chi}^N(y, \tau_N^-), \theta) = \partial \psi(\bar{\chi}^N(y, \tau_N^-), \theta) / \partial \bar{\chi}$, $\bar{\chi}^N = [T^N, \alpha^N, S^{TN,j}, S^{\alpha N,j}]'$ and the explicit form of the function $\psi(\bar{\chi}^N(y, \tau_N^-), \theta)$ is given in the Appendix (A4).

- c) Boundary conditions time $t = \tau_i$, $i = 1, 2, \dots, N - 1$

$$\bar{p}^{Ti}(y, \tau_i^-) = F_T^{i'}(\chi^i(y, \tau_i^-), \chi_0(y)) \bar{p}^{Ti+1}(y, \tau_i^+) \quad (18a)$$

$$\bar{q}^{Ti}(y, \tau_i^-) = F_\alpha^{i'}(\chi^i(y, \tau_i^-), \chi_0(y)) \bar{q}^{Ti+1}(y, \tau_i^+) \quad (18b)$$

$$\bar{p}^{si,j}(y, \tau_i^-) = F_T^{i'}(\chi^i(y, \tau_i^-), \chi_0(y)) \bar{p}^{si+1,j}(y, \tau_i^+) \quad (18c)$$

$$\bar{q}^{si,j}(y, \tau_i^-) = F_\alpha^{i'}(\chi^i(y, \tau_i^-), \chi_0(y)) \bar{q}^{si+1,j}(y, \tau_i^+). \quad (18d)$$

TABLE I
NUMERICAL ALGORITHM

- Chose initial iterate τ_i^0 for $i = 1, \dots, N$ to initialize time vector $[\tau_1, \dots, \tau_N]'$, and chose a termination tolerance σ .
- Set iteration counter $k = 0$.
- While $|J_R^k - J_R^{k-1}| > \sigma$
 - Step 1: For $i = 1$, first spatially discretize the PDEs in (2) and (10) to reduce to set of ODEs and then compute the augmented state $\chi^1(t) = [T^1(t), \alpha^1(t)]'$ and $\chi^{s1}(t) = [S^{T1}(t), S^{\alpha 1}(t)]'$ forward-in-time from $t_0 = 0$ to $t_f = \tau_1$.
 - Step 2: For $i > 1$, to compute $\chi^i(t)$ and $\chi^{si}(t)$ forward-in-time from $t_0 = \tau_1$ to $t_f = \tau_N$, first update the PDEs in (2) and (10) using interface condition in (4) and (12), respectively. Then, spatially discretize the updated PDEs to a set of ODEs and impose the transition constraints in (5) and (13).
 - Step 3: Compute the cost function J_R^k in (14).
 - Step 4: For $i = N$, first spatially discretize the PDEs in (15) and (16) to set of ODEs and then compute the adjoint variables $[\bar{p}^{sN,j}(t), \bar{q}^{sN,j}(t)]'$ and, then solve for $[\bar{p}^{TN}(t), \bar{q}^{\alpha N}(t)]'$ backward-in-time from $t_f = \tau_N$ to $t_0 = \tau_{N-1}$ using (17).
 - Step 5: For $i < N$, to compute adjoint variables backward in time from $t_f = \tau_{N-1}$ to $t_0 = 0$, first spatially discretize the PDEs in (15) and (16) to set of ODEs and impose the adjoint mode transition conditions (18).
 - Step 6: Update the time vector τ_i as follows:
 - $\tau_i^{k+1} = \tau_i^k - \delta_i^k C_i$, and
 - $\tau_N^{k+1} = \tau_N^k - \delta_N^k D$
 for $i = 1, \dots, N - 1$, where δ_i^k and δ_N^k step size parameters that satisfy Armijo's step size condition[46], and $C_i = H_i(\tau_i^-, \bar{\theta}) - H_i(\tau_i^+, \bar{\theta})$ in (19a) and $D = H_N(\tau_i^-, \bar{\theta})$ in (19b).
 - Step 7: if $\tau_i < \tau_{i-1}$, $\tau_i = \tau_{i-1} + c$, where c is a constant real number.
 - Step 8: $k = k + 1$
- End while

Note that the interior adjoint conditions (18) are derived by setting $(F_{\chi\chi}^i = 0)$ for the example condition given in (6).

- d) For $\tau_i, i = 1, 2, \dots, N - 1$, the optimality conditions in (19a) should hold, and for τ_N , (19b) should hold

$$H^i(\tau_i^-, \bar{\theta}) - H^{i+1}(\tau_i^+, \bar{\theta}) = 0 \quad (19a)$$

$$H^N(\tau_N^-, \bar{\theta}) = 0 \quad (19b)$$

where

$$\begin{aligned} H^i(\tau_i^-, \bar{\theta}) &= \int_{\Omega} \left[a \bar{p}^{Ti}(y, \tau_i^-) T_{yy}^i(y, \tau_i^-) + \Upsilon^i(\bar{p}^T, \bar{q}^\alpha) f^i(T^i, \alpha^i, \bar{\theta}) \right. \\ &+ \sum_{j=1}^m \{ a \bar{p}^{si,j}(y, \tau_i^-) S_{yy}^{Ti,j}(y, \tau_i^-) \\ &\left. + \Upsilon^{si,j}(\bar{p}^s, \bar{q}^s) f^{si}(T^i, \alpha^i, S^{Ti,j}, S^{\alpha i,j}, \bar{\theta}) \right] dy. \end{aligned} \quad (20)$$

C. Computation Algorithm

Based on the above necessary conditions for optimality, the steepest descent algorithm can be applied to solve for the optimal layering time control vector $[\tau_1, \dots, \tau_N]'$. Note that some of the necessary conditions involve solving PDEs as well as resolving the interface constraints at a new layer addition. These are addressed in the numerical algorithm provided in Table I.

TABLE II
PARAMETER VALUES USED IN THE SIMULATIONS

SYMBOL	PARAMETER	VALUE
ρ	Density of composite	1.69 g/cm ²
c_p	Specific heat of composite	1.14 J/g °C
k_z	Thermal conductivity of composite	0.0026 W/cm °C
ρ_r	Density of resin	1.1 g/cm ²
h	Convective heat transfer	0.0002 W/cm ² °C
ΔH_r	Polymerization enthalpy of resin	335 J/g
E_1 & E_2	Activation energies	[25.9 & 11.7] KJ/mol
A_1 & A_2	Pre-exponential factors	[0.92 & 0.64] s ⁻¹
R	Gas constant	8.314 J/mol K
s_0	Photoinitiator concentration	0.05 wt%
λ	UV attenuation constant	2 cm ⁻¹
T_∞	Ambient temperature	25 °C
B	Cure kinetics constant	1.22
v_r	Volume fraction of resin	0.6
p & q	Constants exponents	0.86 & 0.87
ϑ	Absorptivity of UV radiation	0.85
α_c	Critical cure level	0.92
ξ	Diffusion constant	159.4

Remark 1: For this numerical algorithm, the PDEs can be transformed to a set of ODEs using a central-in-space finite-difference method. Then, the augmented ODE systems can be solved forward or backward-in-time using Euler's method.

Remark 2: The optimal interlayer hold times (time gaps between new layers) can be computed by taking the differences between successive elements of the computed control vector $[\tau_1, \dots, \tau_N]'$.

IV. RESULTS AND DISCUSSION

In this section, we present the simulation results to demonstrate the feasibility and advantage of the proposed robust optimization scheme by simulating the composite laminate (fiberglass plus unsaturated polyester resin) fabrication process via the layer-by-layer SCC process. Here, we are interested in achieving near-through-cure in all layers at the end of the curing process by optimizing the interlayer hold times. This is described by selecting a nominal terminal cost function g in (13) of the form $g(\chi^N(y, \tau_N^-, \bar{\theta})) = 0.5\{\alpha^N(y, \tau_N^-) - \alpha_d(y)\}^2, y \in [0, N]$.

For the simulation study, we present here the associated thermal, chemical, and material constants for photopolymerization of unsaturated polyester resin, which are extracted from [47] and updated with our own curing experiments [16]. For the fiberglass, E-glass thermal properties such as thermal conductivity ($k_z = 0.012$ W/cm °C), specific heat ($c_p = 0.8$ J/g °C), and density ($\rho = 2.55$ g/cm³) are used. The resin volume fraction is assumed to be 60% for computing the average thermal properties of the composite laminate. The associated parameters used in the simulations are summarized in Table II.

For the process simulation and implementation of the optimization algorithm, a ten-node spatial discretization is adopted for each layer to convert the temperature and sensitivity PDEs and the corresponding adjoint PDEs to a set of ODEs in time. A total of ten layers with a thickness of 1 mm each are considered to fabricate a 10-mm thick composite laminate.

TABLE III
FINAL CURING TIME FOR CONSIDERED CASES

CONSIDERED CASES	FINAL CURING TIMES (S)
Case 1	905
Case 2	905
Case 3	980
Case 4	1082

The desired/target final cure level is specified to be 90% across all layers (desired cure level of $\alpha = 0.9$). A constant UV intensity of 65 mW/cm² is used for the entire curing duration.

We illustrate the advantages of the proposed robust optimization scheme by comparing the results of two robust optimal cases, one nominal optimal case and one nonoptimal case.

- 1) *Case 1:* A nonoptimal approach with equal-interval layering time.
- 2) *Case 2:* Nominal optimized layering time control with robustness measure $\beta = 0$.
- 3) *Case 3:* Robust optimized layering time control with robustness measure $\beta = 5$.
- 4) *Case 4:* Robust optimized layering time control with robustness measure $\beta = 10$.

For the non-optimal case of equal-interval layering time (Case 1), the length of the overall curing time is kept the same as that of the overall curing duration of the nominal optimal case (Case 2). As will be shown in Figs. 6–8, the achieved final cure level distribution with equal-interval layering time (Case 1) is not acceptable; we shall not dwell on this case too much. For the last two robust optimal cases (Cases 3 and 4), the optimization is executed until the robustness term of the cost function defined by system sensitivity reaches near zero. The second case is simulated using nominal optimal layering times as presented in [14], while the third and fourth cases are considered the robust optimization result presented in this paper. The overall curing times computed for each optimization case are summarized in Table III.

The results are presented in two parts. First, we present the spatiotemporal evolutions of both the cure state and the temperature states for the nominal optimization case (Case 2) to illustrate the cure and temperature propagation as the part is built in a layer-by-layer SCC process. We will then evaluate the proposed robust optimization of the layering time control by considering specific parametric uncertainties.

As shown in Fig. 3, complete cure is achieved in all layers by first initiating the cure in the bottom layers and following the SCC process. As the top layers are added and cure with direct UV exposure, the cure initiated in the bottom layers continues to propagate with the attenuated UV radiation reaching there. As a result of optimizing the layering time control (interlayer hold times), the cure in the bottom layers proceeds with the attenuated radiation for an extended length of time while in the top layers it proceeds with less attenuated radiation for shorter times. This differentiation helps to minimize the final cure level deviation across the part. The optimal

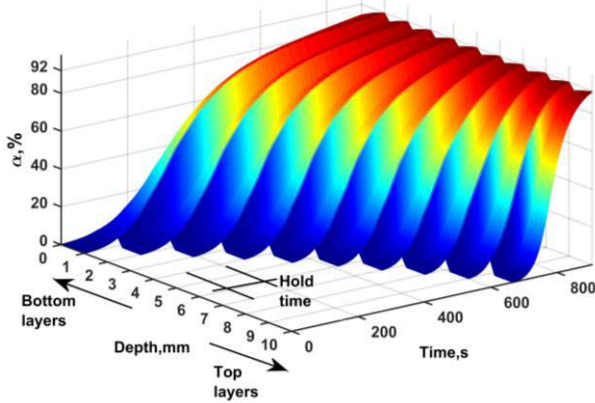


Fig. 3. Cure level profile with nominal optimized layering time control.

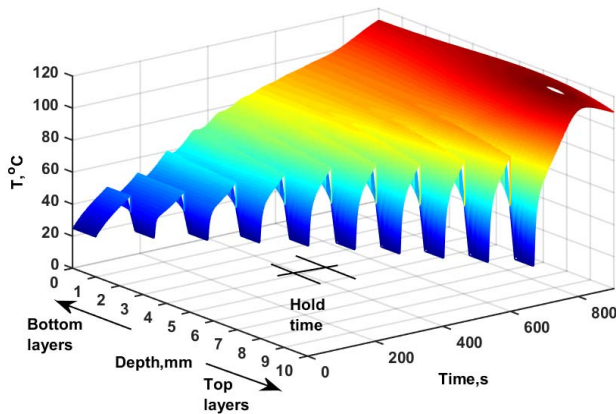


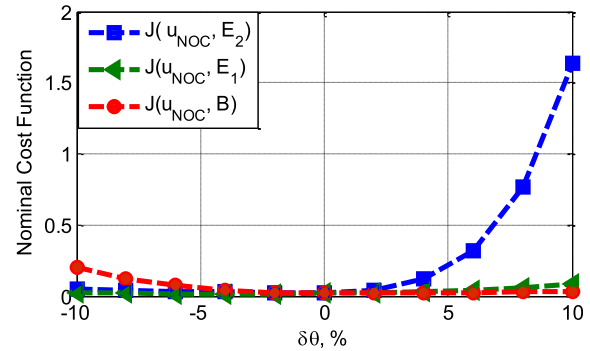
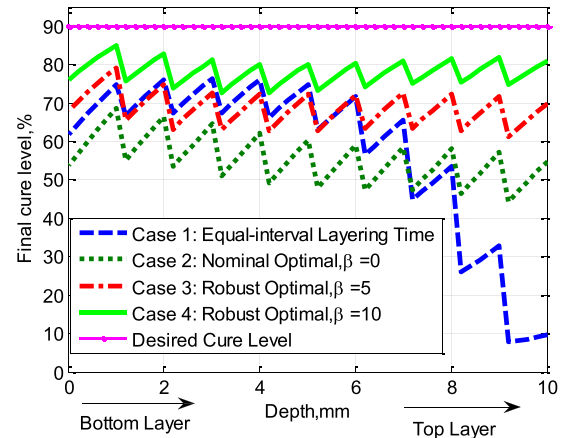
Fig. 4. Temperature profile with nominal optimized layering time control.

interlayer hold times and their trend for this nominally optimal case are shown in Fig. 9, along with the results for the robust optimal cases to be discussed below.

Fig. 4 shows the corresponding temperature evolution during the layer-by-layer UV curing process. After the cure is initiated, the temperature gradually builds up. However, unlike the cure state, after each layer addition the temperature initially decreases before increasing again. This is due to the heat transfer between the new layer (added at ambient conditions) and the previous layers at elevated temperatures. This self-cooling property of the layer-by-layer SSC process by itself may help to reduce the overall curing temperature gradients while processing thick sections.

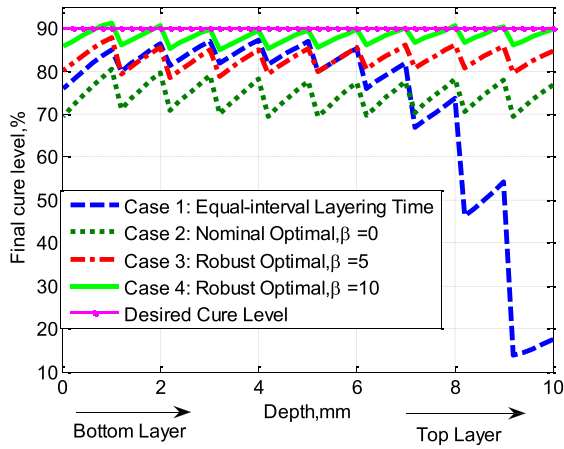
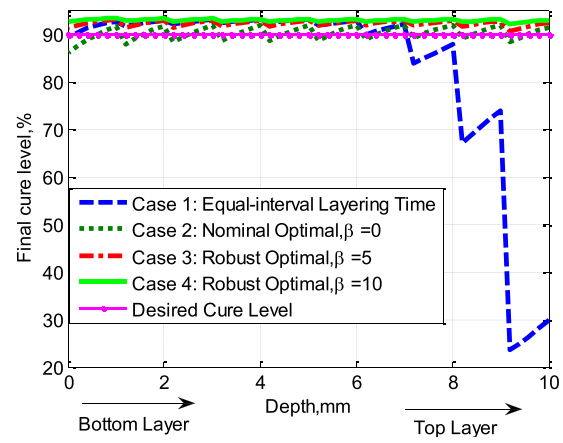
For the robust optimization cases (Cases 3 and 4), we investigated the effect of variations in each component of the uncertain parameter vector $\theta = [E_1, E_2, \bar{B}]'$ on the nominally optimal result. This is experimented by simulation studies that consider a $\pm 10\%$ deviation from nominal for each of the three uncertain parameters. The computed nominal cost function for the different values of the uncertain parameter is plotted in Fig. 5. The parameter variations are considered one at a time on the same nominally optimized layering time control of Case 2.

Fig. 5 shows that the deviation in parameter E_2 has the most significant effect on the nominal cost function compared with

Fig. 5. Nominal cost function for up to 10% deviation of the uncertain parameters (u_{NOC} is nominal control input).Fig. 6. Final cure level profile with +10% parameter deviation in E_2 .

the deviation in the other parameters E_1 and \bar{B} . Furthermore, it is clear from the plot that the cost function changes as the increase and decrease of these factors are not symmetric. This can be explained by the nature of the cure propagation captured by the cure kinetics model in (2). For example, in the case of parameter E_2 , the deviation in the positive direction (increase of E_2 from its nominal value) decreases the cure rate and this causes an incomplete cure and larger deviation of the final cure level as the parameter deviates more. Whereas the deviation in the negative direction increases the cure rate, the rate of this cure rate increment after a critical cure level of $\alpha_c = 0.92$ (which is closer to the desired cure level of $\alpha = 0.9$) is not significant because of the diffusion-controlled effect. As a result, significant changes are not observed in the nominal cost function due to a decrease of E_2 from its nominal value. The same discussion can be extended to the deviations in the other two uncertain parameters. Therefore, for the results presented below, we only consider the uncertainty in the parameter E_2 for the robust optimization cases, specifically its deviation in the positive direction.

As discussed in the Introduction and later shown in Fig. 3, the optimized SCC scheme can be used to achieve the desired cure level with the minimum overall deviation in all the layers ($\leq 5\%$). However, the presence of uncertainty in the process parameters affects this nominal optimization result. As shown in Fig. 6, a +10% deviation in E_2 in the process

Fig. 7. Final cure level profile with +6% parameter deviation in E_2 .Fig. 8. Final cure level profile with 0% parameter deviation in E_2 .

model reduces the nominally optimized result (Case 2) of the final cure level from about 90% (see Fig. 3) to about 55% on average with an overall deviation of more than 15% across layers. On the other hand, with robust optimization that penalizes the sensitivity of the objective function, the cure level deviations in the layers as well as between the desired and achieved final cure level are significantly reduced. With different choices of the robustness measure, $\beta = 5$ (Case 3) and $\beta = 10$ (Case 4), the final cure level of about 70% and 80% are achieved, respectively, with an overall cure level deviation across the part of less than 12% and 7%, respectively.

A similar result presented in Fig. 7 for a +6% deviation in E_2 shows that the desired final cure level of 90% is nearly achieved in all the layers with the robust optimization (Case 4), while the nominal optimization (Case 2) subject to this uncertainty achieves a final cure level of less than 75%. From the results in Figs. 6 and 7, it is clear that by increasing the robustness measure β , the robust performance is improved significantly as the sensitivity of the final cure state is penalized with this measure.

Fig. 8 shows the performance for a 0% deviation in E_2 . In both the cases of robust optimization (Cases 3 and 4), marginal overcure is observed in all the layers, while the nominal optimization (Case 2) is just enough to achieve the desired cure level distribution. The overcure can be explained by the need for longer overall curing times in the robust optimization cases (Table III), which comes about to compensate the degraded cure propagation especially in the case of the positive direction parameter deviations discussed above.

Fig. 9 shows that the control actions (interlayer hold times) for the robust and nominal optimal cases differ but follow a similar trend in all the three optimal cases. They first decrease as the early layers are added from the bottom and then increase for the top layers. The larger hold times computed for the early bottom layers can be explained by the anticipation via optimization of the attenuation of UV radiation in the bottom layers as new layers are added on. The largest hold time for the last and top layer can be explained by the need for bringing the cure level there from zero to the desired level quickly, while the cure level continues to build in the lower layers

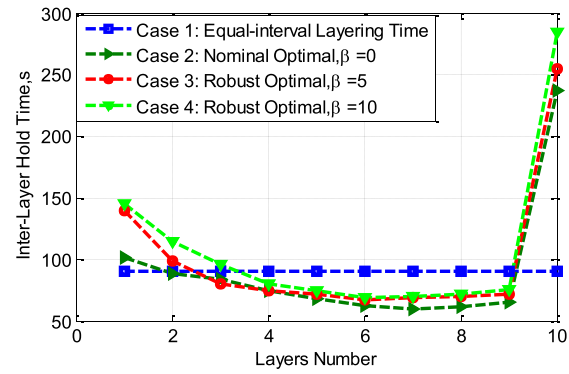
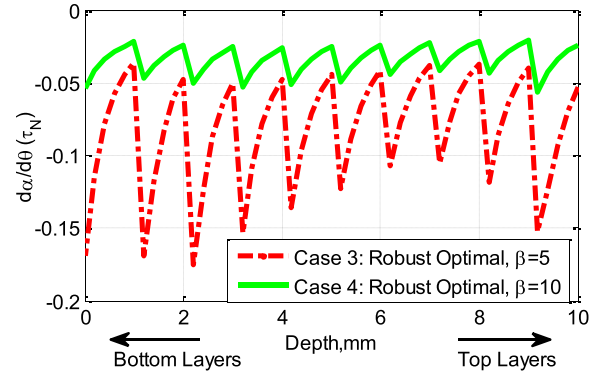


Fig. 9. Optimized interlayer hold times for Cases 2-4.

Fig. 10. Sensitivity of the final cure state for Cases 3 and 4 ($d\alpha/d\theta$ is normalized with respect to its maximum).

with attenuated UV radiation. Particularly, for the robust cases (Cases 3 and 4), relatively larger interlayer hold times are computed to accommodate the possible cure rate degradation due to parameter uncertainty.

Fig. 10 shows the sensitivity of the final cure state with an increment of the robustness measure β . For the considered worst case +10% deviation in E_2 , Fig. 10 also shows that there is still room for further improvement for robust performance by increasing β until the sensitivity of the final cure state to the parameter is eliminated.

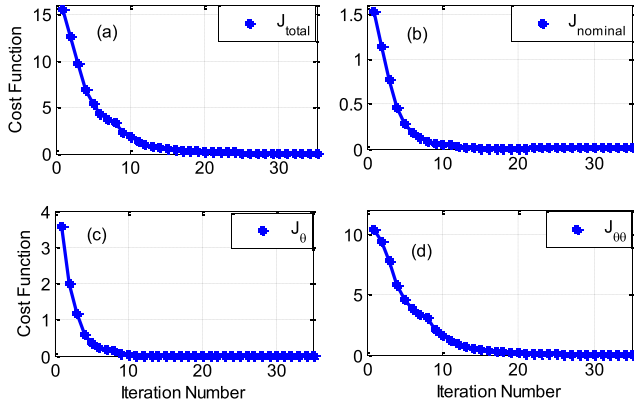


Fig. 11. Convergence of computational algorithm. (a) Total cost. (b) Nominal cost. (c) First-moment sensitivity cost. (d) Second-moment sensitivity cost.

Finally, in Fig. 11, the progresses of different segments of the cost function are shown to comment on the computational algorithm as well as to illustrate its convergence. The robust optimization of the layering control discussed earlier in this paper considers only the first-moment Taylor's approximation of the sensitivity of the cost function to parametric uncertainty given in (9), and then formulates the first moment sensitivity dynamics and the corresponding adjoint system. However, for the specific structure of the cost function considered in this paper, we found that the consideration of the second-moment Taylor's approximation of the sensitivity improves the performance of the robust optimization significantly. The specific forms of the nominal cost function as well as the first moment and the second moment are given in (B1). The additional auxiliary sensitivity dynamics associated with second-moment sensitivity are given in (B2).

As shown in Fig. 11, the cost associated with the first-moment sensitivity [Fig. 11(c)] converges close to zero in a few iterations (less than ten) and stops changing, while the cost with second moment [Fig. 11(d)] continues to improve with more iteration. This is because the second moment introduces additional quadratic term of final cure state sensitivity that reduces smoothly with increasing iteration. The first moment only consists of the product of the actual cure state deviation and cure state sensitivity, which prematurely vanishes as the actual cure state deviation approaches zero before the cure state sensitivity goes to zero. That is, a local optimal solution is encountered when only the first moment was retained.

It should be noted that the improvement of the performance with the second moment cost sensitivity considerations comes with the added complexity and increase in the computational burden. However, since these computations are done offline to find robust control sequences (layering times), these computations are very feasible. For the numerical results presented in Figs. 6–8, the CPU time for the optimization algorithm was of the order of 1.5 h (on a high-end 2012 Dell laptop: Latitude E6520, intel corei7-2640M, 2.8 GHZ CPU, 8 GB RAM, 500 GB Hard Disk), with the code implemented in MATLAB, for a model with ten-node discretization per layer and consideration of the second-order moment for robustness. The discretization number was held the same for all dynamics

including process state dynamics, sensitivity dynamics, and adjoint system dynamics. Of course, the CPU time can be improved, for example, by considering different discretization sizes for the state dynamics (fine discretization) and the adjoint system dynamics (coarse discretization).

V. CONCLUSION

This paper presented a systematic layering control and a robust optimization scheme for a layer-by-layer deposition and curing process by modeling the process as a multimode hybrid dynamic system with a predefined mode sequence and increasing spatial domain. The hybrid interpretation of the layering and curing sequence has been detailed by defining INTCs and mode-transition operators for the layer-by-layer deposition process. Then, the layering times (the interlayer times) are posed as the control variables to be selected optimally so as minimize final cure level deviation in a multilayer thick part in the presence of parameter uncertainties. The necessary optimality conditions that can be used to compute the interlayer hold times were derived by defining the sensitivity of the objective function as a robustness measure and considering it as an additional cost function. The robust optimization problem is posed and solved by adjoining the corresponding system sensitivity and state dynamics as well as the INTCs and mode-transition operators within the hybrid framework.

This paper included detailed simulation results and analysis of the proposed schemes using a recently verified model for a UV-curing process. The simulations focused on a thick composite laminate processing application and illustrated the advantages of the robust hybrid system optimization schemes in achieving robust process control via the optimal-inter layer hold times in the presence of uncertain parameters. Computational aspects have also been discussed, where it is argued that for the offline robust optimization of the layering times, the convergence of the outlined algorithm can be refined by adding second-moment sensitivity costs to the objective and modify the auxiliary sensitivity dynamics accordingly.

APPENDIX A DERIVATION OF NECESSARY CONDITIONS FOR OPTIMALITY

We use Lagrange multipliers to adjoin the state dynamics (2), sensitivity dynamics (10), and corresponding transition constraints (5) and (13), respectively, to the cost functions in (14) as defined in Section III. The augmented optimal cost is given by

$$\begin{aligned}
 J = & \sum_{i=1}^N \int_{\tau_{i-1}}^{\tau_i} \int_{\Omega} \mathcal{L}^i(\bar{p}^{Ti}, \bar{p}^{si,j}, \bar{q}^{ai}, \bar{q}^{si,j}, T^i, \alpha^i, S^{Ti,j}, S^{ai,j}) dy dt \\
 & + \sum_{i=1}^{N-1} \int_{\Omega} \mathcal{M}^i(\mu^i, \mu^{si,j}, \chi^i, \chi^{i+1}, \chi^{si,j}, \tau_i) dy + \int_{\Omega} \psi(\bar{\chi}^N, \theta) dy
 \end{aligned} \tag{A1}$$

where

$$\begin{aligned} \mathcal{L}^i(\bar{p}^{Ti}, \bar{p}^{si,j}, \bar{q}^{ai}, \bar{q}^{si,j}, T^i, \alpha^i, S^{Ti,j}, S^{ai,j}) \\ = -\bar{p}^{Ti}(T^i - aT_{yy}^i) - \bar{q}^{ai}\alpha^i + \Upsilon^i(\bar{p}^T, \bar{q}^a)f^i(T^i, \alpha^i, \theta) \\ + \sum_{j=1}^m \left\{ -\bar{p}^{si,j}(S^{Ti,j} - aS_{yy}^{Ti,j}) - \bar{q}^{si,j}S^{ai,j} \right. \\ \left. + \Upsilon^{si,j}(\bar{p}^s, \bar{q}^s)f^{si}(T^i, \alpha^i, S^{Ti,j}, S^{ai,j}, \theta) \right\} \quad (\text{A2}) \end{aligned}$$

$$\begin{aligned} \mathcal{M}^i(\mu^i, \mu^{si,j}, \chi^i, \chi^{i+1}, \chi^{si,j}, \tau_i) \\ = \mu^i(\tau_i^-)[F^i(\chi^i(\tau_i^-), \chi_0) - \chi^{i+1}(\tau_i^+)] \\ + \sum_{j=1}^m \mu^{si,j}(\tau_i^-)[F_\chi^i(\chi^i(\tau_i^-), \chi_0)S^{\chi^{i,j}}(\tau_i^-) - S^{\chi^{i+1,j}}(\tau_i^+)] \quad (\text{A3}) \end{aligned}$$

$$\begin{aligned} \psi(\bar{\chi}^N, \bar{\theta}) = g(\chi^N(y, \tau_N^-), \bar{\theta}) \\ + \sum_{i=1}^m \beta_j \frac{\partial g(\chi^N(y, \tau_N^-), \bar{\theta})}{\partial \chi^N} S^{\chi^{N,j}}(\zeta, \tau_N^-) \\ \times \int_{\Omega_\zeta} \frac{\partial g(\chi^N(\zeta, \tau_N^-), \bar{\theta})}{\partial \chi^N} S^{\chi^{N,j}}(\zeta, \tau_N^-) d\zeta, \\ \Omega_\zeta \in [0, N]. \quad (\text{A4}) \end{aligned}$$

The function ψ in (A4) contains a cost function that involves square of the integral from (13) written in the form: $[\int_0^l f(x)dx]^2 = \int_0^l \{f(x) \int_0^l f(y)dy\}dx$ to simplify the derivation.

For brevity, the spatial and temporal indices of the state are dropped in (A1)–(A4) and in the following derivation, except at the switching node τ_i .

To compute the gradient of the robust optimal cost, we perturb the variables in (A1) in such a way that $\tau_i \rightarrow \tau_i + \delta\tau_i$, $T^i \rightarrow T^i + \delta T^i$, $\alpha^i \rightarrow \alpha^i + \delta\alpha^i$, $S^{Ti} \rightarrow S^{Ti} + \delta S^{Ti}$ and $S^{ai} \rightarrow S^{ai} + \delta S^{ai}$. Substituting the defined perturbation into (A1) and taking first-order Taylor's approximation and subtracting (A1) from the perturbed result, we obtain the gradient of the optimal cost

$$\begin{aligned} \delta J = \sum_{i=1}^N \int_{\tau_{i-1}}^{\tau_i} \int_{\Omega} \\ \times \delta \mathcal{L}^i(\bar{p}^{Ti}, \bar{p}^{si,j}, \bar{q}^{ai}, \bar{q}^{si,j}, \delta T^i, \delta \alpha^i, \delta S^{Ti,j}, \delta S^{ai,j}) dy dt \\ + \sum_{i=1}^{N-1} \int_{\Omega} \delta \mathcal{M}^i(\mu^i, \mu^{si,j}, \delta \chi^i, \delta \chi^{i+1}, \delta \chi^{si,j}, \delta \tau_i) dy \\ + \int_{\Omega}^N [\psi_{\bar{\chi}^N} \delta \bar{\chi}^N(\tau_N^-) + \psi_{\bar{\chi}^N} \bar{\chi}_i^N(\tau_N^-) \delta \tau_N] dy \quad (\text{A5}) \end{aligned}$$

where

$$\begin{aligned} \delta \mathcal{L}^i(\bar{p}^{Ti}, \bar{p}^{si,j}, \bar{q}^{ai}, \bar{q}^{si,j}, \delta T^i, \delta \alpha^i, \delta S^{Ti,j}, \delta S^{ai,j}) \\ = -\bar{p}^{Ti}(\delta T^i - a\delta T_{yy}^i) - \bar{q}^{ai}\delta \alpha^i + \Upsilon^i(\bar{p}^T, \bar{q}^a) \\ \times [f_T^i \delta T^i + f_\alpha^i \delta \alpha^i] + \sum_{j=1}^m \left\{ -\bar{p}^{si,j} * (\delta S^{Ti,j} - a\delta S_{yy}^{Ti,j}) \right. \\ \left. - \bar{q}^{si,j} \delta S^{ai,j} + \Upsilon^{si,j}(\bar{p}^s, \bar{q}^s)[f_T^{si} \delta T^i + f_\alpha^{si} \delta \alpha^i \right. \\ \left. + f_T^{si} \delta S^{Ti,j} f_\alpha^{si} \delta S^{ai,j} \right\} \quad (\text{A6}) \end{aligned}$$

$$\begin{aligned} \delta \mathcal{M}^i(\mu^i, \mu^{si,j}, \delta \chi^i, \delta \chi^{i+1}, \delta \chi^{si,j}, \delta \tau_i) \\ = \mu^i(\tau_i^-)[(F_\chi^i \chi^i(\tau_i^-) - \chi^{i+1}(\tau_i^+))\delta \tau_i \\ + F_\chi^i \delta \chi^i(\tau_i^-) - \delta \chi^{i+1}(\tau_i^+)] + \sum_{j=1}^m \mu^{si,j}(\tau_i^-) \\ * [(F_\chi^i S^{si,j}(\tau_i^-) - S^{si,j}(\tau_i^+))\delta \tau_i \\ + F_\chi^i \delta S^{si,j}(\tau_i^-) - \delta S^{si,j}(\tau_i^+)]. \quad (\text{A7}) \end{aligned}$$

In (A5), we impose three considerations.

- 1) The change in state variables due to a change in the switching time and final time is approximated by the linear relation (e.g., $F^i(\chi^i(\tau_i + \delta\chi^i), \chi_0) = F^i(\chi^i(\tau_i^-), \chi_0) + F_T^i \chi^i(\tau_i^-) \delta\tau_i$ [29]).
- 2) In the open intervals $(\tau_i \tau_i + \delta\tau_i)$ and $(\tau_{i-1} \tau_{i-1} + \delta\tau_{i-1})$, the dynamic constraints such as $T_{ii} - aT_{yyi} - b(y)f^i(T^i, \alpha^i, \theta)$ are set to zero.
- 3) To simplify the derivation, the transition operator for the sensitivity dynamic F_χ^i is assumed to be constant matrices [for example, condition in (6)].

Using integration by parts for the integral terms that contain time and space derivatives, and substituting the perturbed BCs from (2), part of the integral terms in (A6) read

$$\begin{aligned} \sum_{i=1}^N \int_{\tau_{i-1}}^{\tau_i} \int_{\Omega^i} [\bar{p}^{Ti}(\delta T^i - a\delta T_{yy}^i) + \bar{q}^{ai}\delta \alpha^i] dy dt \\ = \sum_{i=1}^N \int_{\Omega^i} \{ \bar{p}^{Ti} \delta T^i |_{\tau_i} - \bar{p}^{Ti} \delta T^i |_{\tau_{i-1}} \\ + \bar{q}^{ai} \delta \alpha^i |_{\tau_i} - \bar{q}^{ai} \delta \alpha^i |_{\tau_{i-1}} \} dy \\ - \int_{\tau_{i-1}}^{\tau_i} \{ [c\bar{p}^{Ti}(il) - \bar{p}_y^{Ti}(il)] \delta T^i(il) + a\bar{p}_y^{Ti}(0) \delta T^i(0) \} dt \\ - \sum_{i=1}^N \int_{\tau_{i-1}}^{\tau_i} \int_{\Omega^i} [\delta T^i(\bar{p}_t^{Ti} + a\bar{p}_{yy}^{Ti}) + \bar{q}_t^{ai} \delta \alpha^i] dy dt. \quad (\text{A8}) \end{aligned}$$

We further simplify the terms in (A6) and partly in (A8), setting $\delta\tau_0$, δT_0 and $\delta\alpha_0$ to zero for fixed initial time and states. An example case is given as

$$\sum_{i=1}^N \int_{\Omega} \bar{p}^{Ti} \delta T^i |_{\tau_i} dy = \sum_{i=1}^{N-1} \int_{\Omega} \bar{p}^{Ti} \delta T^i dy + \int_{\Omega} \bar{p}^{TN} \delta T^N dy. \quad (\text{A9})$$

Substituting (A9) into (A8), and substituting the simplified results back into (A5) and reorganizing terms, we arrive at the adjoint equations of the coupled PDE–ODE system given in (15)–(18). Then setting the remaining terms to zero to make $\delta J = 0$, we arrive at the necessary condition for optimality given by (19).

APPENDIX B SYSTEM SENSITIVITY DYNAMICS WITH CONSIDERATION OF SECOND MOMENT ROBUSTNESS

To improve the robustness performance of the proposed scheme, the cost function given in (14) can be modified to

include the second-moment robustness term

$$\begin{aligned}
J(u, \theta) &= \underbrace{\int_{\Omega^N} g(\chi^N(y, \tau_N^-), \bar{\theta}) dy}_{\text{Nominal cost}} \\
&+ \underbrace{\sum_{j=1}^m \beta_j \left[\int_{\Omega^N} \frac{\partial g(\chi^N(y, \tau_N^-), \bar{\theta})}{\partial \chi^N} S^{\chi^N, j}(y, \tau_N^-) dy \right]^2}_{\text{First moment sensitivity cost}} \\
&+ \underbrace{\left[\frac{1}{2} \int_{\Omega^N} \left\{ [S^{\chi^N, j}(y, \tau_N^-)]^2 + \frac{\partial g(\chi^N(y, \tau_N^-), \bar{\theta})}{\partial \chi^N} S_{\theta}^{\chi^N, j}(y, \tau_N^-) \right\} dy \right]^2}_{\text{Second moment sensitivity cost}}
\end{aligned} \tag{B1}$$

where $S_{\theta}^{\chi^N, j} = \partial S^{\chi^N, j} / \partial \theta_j$.

The corresponding system sensitivity dynamics with second-moment sensitivity consideration are, for $j = 1, \dots, m$

$$\begin{aligned}
S_{\theta t}^{T, i, j}(y, t) &= a S_{\theta y}^{T, i, j}(y, t) + b(y) \\
&\times \{ f_T^{s, i} S_i^T(y, t) + f_{\alpha}^{s, i} S^{\alpha, i, j}(y, t) + f_{\theta \alpha}^{i, j} S^{\alpha, i, j}(y, t) \\
&+ f_{\theta T}^{i, j} S_i^T(y, t) + f_T^{i, j} S_{\theta}^{T, i, j}(y, t) + f_{\alpha}^{i, j} S_{\theta}^{\alpha, i, j}(y, t) \\
&+ f_{\theta \theta}^{i, j} \} \text{ in } \Omega_{\tau}^i \tag{B2a}
\end{aligned}$$

$$S_{\theta y}^{T, i, j}(il, t) = c S_{\theta}^{T, i, j}(il, t) \text{ on } \Gamma_1^i \tag{B2b}$$

$$S_{\theta y}^{T, i, j}(0, t) = 0 \text{ on } \Gamma_2^i \tag{B2c}$$

$$\begin{aligned}
S_{\theta t}^{\alpha, i, j}(y, t) &= d(y) \{ f_T^{s, i} S_i^T(y, t) + f_{\alpha}^{s, i} S^{\alpha, i, j}(y, t) \\
&+ f_{\theta \alpha}^{i, j} S^{\alpha, i, j}(y, t) + f_{\theta T}^{i, j} S_i^T(y, t) + f_T^{i, j} S_{\theta}^{T, i, j}(y, t) \\
&+ f_{\alpha}^{i, j} S_{\theta}^{\alpha, i, j}(y, t) + f_{\theta \theta}^{i, j} \} \text{ in } \Omega_{\tau}^i. \tag{B2d}
\end{aligned}$$

The associated sensitivity of the INTCs and mode transition operators can be derived taking partial derivative with respect to θ on both sides of (11) and (12), respectively. For the implementation of the numerical algorithm, the corresponding adjoint system is derived in the same way as in Appendix A by adjoining the additional sensitivity dynamics (B2) and the associated transition constraints.

REFERENCES

- [1] G. Tapia and A. Elwany, "A review on process monitoring and control in metal-based additive manufacturing," *J. Manuf. Sci. Eng.*, vol. 136, no. 6, p. 060801, 2014.
- [2] *Measurement Science Roadmap for Metal-Based Additive Manufacturing*, Nat. Inst. Standards Technol., Columbia, MD, USA, 2013, http://www.nist.gov/el/isd/upload/NISTAdd_Mfg_Report_FINAL-2.pdf
- [3] N. Guo and M. C. Leu, "Additive manufacturing: Technology, applications and research needs," *Frontiers Mech. Eng.*, vol. 8, no. 3, pp. 215–243, 2013.
- [4] K. Zeng, D. Pal, and B. Stucker, "A review of thermal analysis methods in laser sintering and selective laser melting," in *Proc. Solid Freeform Fabrication Symp.*, Austin, TX, USA, 2012, pp. 796–814.
- [5] S. L. Campanelli, G. Cardano, R. Giannoccaro, A. D. Ludovico, and E. L. J. Bohez, "Statistical analysis of the stereolithographic process to improve the accuracy," *Comput.-Aided Design*, vol. 39, no. 1, pp. 80–86, 2007.
- [6] K. Zeng *et al.*, "Layer by layer validation of geometrical accuracy in additive manufacturing processes," in *Proc. Solid Freeform Fabrication Symp.*, Austin, TX, USA, 2013, pp. 12–14.
- [7] H. Wenbin, L. Y. Tsui, and G. Haiqing, "A study of the staircase effect induced by material shrinkage in rapid prototyping," *Rapid Prototyping J.*, vol. 11, no. 2, pp. 82–89, 2005.
- [8] X. Wang, "Calibration of shrinkage and beam offset in SLS process," *Rapid Prototyping J.*, vol. 5, no. 3, pp. 129–133, 1999.
- [9] D. Hu and R. Kovacevic, "Sensing, modeling and control for laser-based additive manufacturing," *Int. J. Mach. Tools Manuf.*, vol. 43, no. 1, pp. 51–60, 2003.
- [10] X. Cao and B. Ayalew, "Multivariable predictive control of laser-aided powder deposition processes," in *Proc. Amer. Control Conf.*, Chicago, IL, USA, Jul. 2015, pp. 3625–3630.
- [11] Y. C. Cho, W. H. Kwon, and C. G. Cassandras, "Optimal control for steel annealing processes as hybrid systems," in *Proc. 39th IEEE Conf. Decision Control*, Sydney, NSW, Australia, Dec. 2000, pp. 540–545.
- [12] P. Manon, C. Valentin-Roubinet, and G. Gilles, "Optimal control of hybrid dynamical systems: Application in process engineering," *Control Eng. Pract.*, vol. 10, no. 2, pp. 133–149, 2002.
- [13] A. Yebe and B. Ayalew, "Optimal layering time control for stepped-concurrent radiative curing process," *J. Manuf. Sci. Eng.*, vol. 137, no. 1, p. 011020, 2015.
- [14] A. Yebe and B. Ayalew, "A hybrid modeling and optimal control framework for layer-by-layer radiative processing of thick sections," in *Proc. Amer. Control Conf.*, Chicago, IL, USA, 2015, pp. 3619–3624.
- [15] A. Endrueit, M. S. Johnson, and A. C. Long, "Curing of composite components by ultraviolet radiation: A review," *Polym. Compos.*, vol. 27, no. 2, pp. 119–128, Apr. 2006.
- [16] A. Yebe, B. Ayalew, and S. Pilla, "Control-oriented model verification for UV processing of composite laminate," *Soc. Adv. Mater. Process Eng.*, Baltimore, MD, USA, May 2015.
- [17] H. Zhang and M. R. James, " L^{∞} bounded robust control for hybrid systems," in *Proc. 45th IEEE Conf. Decision Control*, San Diego, CA, USA, Dec. 2006, pp. 4801–4806.
- [18] J. A. Ball, J. Chudoung, and M. V. Day, "Robust optimal switching control for nonlinear systems," *SIAM J. Control Optim.*, vol. 41, no. 3, pp. 900–931, 2002.
- [19] M. Alamir and I. Balloul, "Robust constrained control algorithm for general batch processes," *Int. J. Control*, vol. 72, no. 14, pp. 1271–1287, 1999.
- [20] J. Darlington, C. C. Pantelides, B. Rustem, and B. A. Tanyi, "Decreasing the sensitivity of open-loop optimal solutions in decision making under uncertainty," *Eur. J. Oper. Res.*, vol. 121, no. 2, pp. 343–362, 2000.
- [21] D. L. Ma, S. H. Chung, and R. D. Braatz, "Worst-case performance analysis of optimal batch control trajectories," *AIChE J.*, vol. 45, no. 7, pp. 1469–1476, 1999.
- [22] Z. K. Nagy and R. D. Braatz, "Open-loop and closed-loop robust optimal control of batch processes using distributional and worst-case analysis," *J. Process Control*, vol. 14, no. 4, pp. 411–422, 2004.
- [23] B. Rustem, "Robust optimal policy methods for nonlinear models," in *Proc. 28th IEEE Conf. Decision Control*, Tampa, FL, USA, Dec. 1989, pp. 2050–2055.
- [24] B. Srinivasan and D. Bonvin, "Dynamic optimization under uncertainty via NCO tracking: A solution model approach," in *Proc. BatchPro Symp.*, 2004, pp. 17–35.
- [25] D. Ruppen, D. Bonvin, and D. W. T. Rippin, "Implementation of adaptive optimal operation for a semi-batch reaction system," *Comput. Chem. Eng.*, vol. 22, nos. 1–2, pp. 185–199, 1998.
- [26] J. W. Helton and M. R. James, *Extending H^{∞} Control to Nonlinear Systems: Control of Nonlinear Systems to Achieve Performance Objectives*. Philadelphia, PA, USA: SIAM, 1999.
- [27] M. Krothapally, J. C. Cockburn, and S. Palanki, "Sliding mode control of I/O linearizable systems with uncertainty," *ISA Trans.*, vol. 37, no. 4, pp. 313–322, 1998.
- [28] R. Loxton, K. L. Teo, and V. Rehbock, "Robust suboptimal control of nonlinear systems," *Appl. Math. Comput.*, vol. 217, no. 14, pp. 6566–6576, 2011.
- [29] A. M. Bayen, R. L. Raffard, and C. J. Tomlin, "Network congestion alleviation using adjoint hybrid control: Application to highways," in *Hybrid Systems: Computation and Control*. Berlin, Germany, Springer, 2004, pp. 95–110.
- [30] X. Xu and P. J. Antsaklis, "Optimal control of switched systems based on parameterization of the switching instants," *IEEE Trans. Autom. Control*, vol. 49, no. 1, pp. 2–16, Jan. 2004.
- [31] E. I. Verriest, "Pseudo-continuous multi-dimensional multi-mode systems," *Discrete Event Dyn. Syst.*, vol. 22, no. 1, pp. 27–59, 2012.
- [32] K. Gokbayrak and C. G. Cassandras, "A hierarchical decomposition method for optimal control of hybrid systems," in *Proc. 39th IEEE Conf. Decision Control*, Dec. 2000, pp. 1816–1821.
- [33] Y. Wardi, P. Twu, and M. Egerstedt, "On-line optimal timing control of switched systems," in *Proc. 49th IEEE Conf. Decision Control (CDC)*, Dec. 2010, pp. 2137–2142.

- [34] M. B. Giles and N. A. Pierce, "An introduction to the adjoint approach to design," *Flow, Turbulence Combustion*, vol. 65, nos. 3–4, pp. 393–415, 2000.
- [35] H. J. Pesch, A. Rund, W. von Wahl, and S. Wendl, "On some new phenomena in state-constrained optimal control if ODEs as well as PDEs are involved," *Control Cybern.*, vol. 39, no. 3, pp. 647–660, 2010.
- [36] S. Wendl, H. J. Pesch, and A. Rund, "On a state-constrained PDE optimal control problem arising from ODE-PDE optimal control," in *Recent Advances in Optimization and Its Applications in Engineering*. Berlin, Germany, Springer, 2010, pp. 429–438.
- [37] S. Wendl, "On a prototype of an optimal control problem governed by ordinary and partial differential equations," Ph.D. dissertation, Univ. Bayreuth, Bayreuth, Germany, 2014.
- [38] M. F. Perry and G. W. Young, "A mathematical model for photopolymerization from a stationary laser light source," *Macromolecular Theory Simul.*, vol. 14, no. 1, pp. 26–39, 2005.
- [39] P. J. da Silva Bártolo, "Optical approaches to macroscopic and microscopic engineering," Ph.D. dissertation, Univ. Reading, Reading, U.K., 2001.
- [40] S. Li and L. Petzold, "Adjoint sensitivity analysis for time-dependent partial differential equations with adaptive mesh refinement," *J. Comput. Phys.*, vol. 198, no. 1, pp. 310–325, 2004.
- [41] X. Xu and P. J. Antsaklis, "Results and perspectives on computational methods for optimal control of switched systems," in *Hybrid Systems: Computation and Control*. Berlin, Germany, Springer, 2003, pp. 540–555.
- [42] T. R. Mehta, D. Yeung, E. I. Verriest, and M. Egerstedt, "Optimal control of multi-dimensional, hybrid ice-skater model," in *Proc. Amer. Control Conf.*, New York, NY, USA, 2007, pp. 2787–2792.
- [43] J. Liu, K. Zhang, C. Sun, and H. Wei, "Second order transition-time optimization for switched dynamical systems," in *Proc. 32nd Chin. Control Conf. (CCC)*, 2013, pp. 2382–2386.
- [44] X. Xu and P. J. Antsaklis, "Optimal control of switched systems via non-linear optimization based on direct differentiations of value functions," *Int. J. Control*, vol. 75, nos. 16–17, pp. 1406–1426, 2002.
- [45] D. E. Kirk, *Optimal Control Theory: An Introduction*. Mineola, NY, USA: Dover, 2004.
- [46] L. Armijo, "Minimization of functions having Lipschitz continuous first partial derivatives," *Pacific J. Math.*, vol. 16, no. 1, pp. 1–3, 1966.
- [47] J. M. Matias, P. J. Bartolo, and A. V. Pontes, "Modeling and simulation of photofabrication processes using unsaturated polyester resins," *J. Appl. Polym. Sci.*, vol. 114, no. 6, pp. 3673–3685, 2009.



Adamu Yebi (M'14) received the B.S. degree in mechanical engineering from Bahir Dar University, Bahir Dar, Ethiopia, and the M.S. degree in sustainable energy engineering and mechanical design from the Royal Institute of Technology, Stockholm, Sweden, in 2011, and Addis Ababa University, Addis Ababa, Ethiopia, in 2010, and the Ph.D. degree in automotive engineering from Clemson University, Clemson, SC, USA, in 2015.

He is currently a Post-Doctoral Research Associate with the Powertrain Research Group, International Center for Automotive Research, Clemson University. His current research interests include dynamic modeling, advanced controls, estimation, optimization, automation and testing for automotive-related applications, and advanced light weight manufacturing.

Dr. Yebi is a member of the American Society of Mechanical Engineers.



Beshah Ayalew (M'15) received the M.S. and Ph.D. degrees in mechanical engineering from Pennsylvania State University, State College, PA, USA, in 2000 and 2005, respectively.

He is currently an Associate Professor of Automotive Engineering and the Director of the DOE GATE Center of Excellence in Sustainable Vehicle Systems with the Clemson University–International Center for Automotive Research, Greenville, SC, USA. His current research interests include control systems and dynamics with applications in manufacturing processes, vehicles, and energy systems.

Dr. Ayalew is an Active Member of IEEE's Control Systems Society, ASME's Vehicle Design Committee, and SAE. He received the SAE's Ralph R. Teetor Educational Award in 2014, the Clemson University Board of Trustees Award for Faculty Excellence in 2012, the NSF CAREER Award in 2011, and the Penn State Alumni Association Dissertation Award in 2005.